JGR Atmospheres

RESEARCH ARTICLE
10.1029/2021JD034830

Key Points:

- The inclusion of the 1991 Pinatubo eruption improves the skill of GEOS-S2S forecasting hemispheric temperature and precipitation rates
- The inclusion of Pinatubo strengthens the forecasted El Niño beyond observations
- Pinatubo does not significantly modify the forecasts of temperatures and precipitation in most extratropical regions

Supporting Information:

Supporting Information may be found in the online version of this article.

Correspondence to:

V. Aquila,
aquila@american.edu

Citation:

Aquila, V., Baldwin, C., Mukherjee, N., Hackert, E., Li, F., Marshak, J., et al. (2021). Impacts of the eruption of Mount Pinatubo on surface temperatures and precipitation forecasts with the NASA GEOS subseasonal-to-seasonal system. *Journal of Geophysical Research: Atmospheres*, *126*, e2021JD034830. https://doi.org/10.1029/2021JD034830

Received 25 FEB 2021
Accepted 19 JUL 2021

Author Contributions:

Formal analysis: Valentina Aquila, Nikita Mukherjee
Investigation: Valentina Aquila
Methodology: Valentina Aquila
Supervision: Valentina Aquila
Visualization: Valentina Aquila, Colleen Baldwin
Writing – original draft: Valentina Aquila

Impacts of the Eruption of Mount Pinatubo on Surface Temperatures and Precipitation Forecasts With the NASA GEOS Subseasonal-to-Seasonal System

Valentina Aquila[1], Colleen Baldwin[1], Nikita Mukherjee[1,2], Eric Hackert[3], Feng Li[4], Jelena Marshak[3], Andrea Molod[3], and Steven Pawson[3]

[1]Department of Environmental Science, American University, Washington, DC, USA, [2]Science Systems and Applications, Inc., Lanham, MD, USA, [3]Global Modeling Assimilation Office, NASA Goddard Space Flight Center, Greenbelt, MD, USA, [4]Goddard Earth Sciences Technology and Research, University Space Research Association, Columbia, MD, USA

Abstract A contemporary seasonal forecasting system is used to study the impacts of a volcanic sulfate injection into the stratosphere on the seasonal forecasts for surface temperatures, the El Niño Southern Oscillation (ENSO), and precipitation. The focus is a case study of the June 1991 eruption of Mt. Pinatubo, Philippines and the period from July 1991 to February 1992. Version 2 of the Goddard Earth Observing System (GEOS) subseasonal-to-seasonal (S2S) forecasting system is used in this study. GEOS-S2S includes the GOddard Chemistry, Aerosols, Radiation and Transport (GOCART) aerosol module, which allows to prognostically simulate aerosol distributions. GOCART is coupled to the radiation and cloud modules to include the impact of the eruption on forecasted radiation and precipitation. The coupled GEOS-S2S system was initialized in May 1991 with fields based on observations to produce ten-member 9-month forecasts with and without the volcanic sulfur injection. The results of these ensemble experiments demonstrate that including Mt. Pinatubo in seasonal forecasts would improve the forecasts of the 1991–1992 global mean temperature and precipitation but worsen the forecast of ENSO by strengthening of El Niño beyond what showed in observations. Most significant changes in the forecasts of temperatures and precipitation are limited to the tropics. The only land area where the inclusion of Pinatubo significantly lowered the forecasted precipitation is tropical Africa.

1. Introduction

Large explosive volcanic eruptions can increase the stratospheric aerosol load by orders of magnitude and impact the climate at a global scale (Robock, 2000). Such eruptions inject sulfur dioxide (SO_2) above the tropopause, where it nucleates and condenses to form sulfate aerosols. These aerosols scatter shortwave radiation, cooling the Earth's surface, and absorb infrared and near-infrared radiation, warming the stratosphere. The resulting net negative radiative forcing leads to a cooling of the global mean surface temperature, which has been detected in observations (e.g., Robock & Mao, 1995; Santer et al., 2014). To date, the largest volcanic eruption to be extensively characterized using satellite observations is that of Mt. Pinatubo, Philippines, on June 15, 1991. Volcanic aerosols from Mt. Pinatubo reached up to 30 km altitude (McCormick & Veiga, 1992; Thomason, 1992) and were still detected in the atmosphere five years after the eruption (McCormick et al., 1995; Thomason et al., 2008).

Data from the Microwave Sounding Unit (Christy et al., 2000) show that the cooling of the global mean temperature peaked at about −0.5 K about 18 months after the eruption (Soden, 2002). Using regression analysis, Gu and Adler (2011) calculated that, once eliminated the impact of the 1991–1992 El Niño, the Pinatubo-induced anomaly was about −0.6 K, even larger than the observed cooling. On the other hand, Robock and Mao (1995), Lean and Rind (2008), and Canty et al. (2013) concluded that the eruption was responsible only for −0.2, −0.14, and −0.25 K of cooling, respectively. Climate models generally reproduce the global cooling, even if disagree on the exact magnitude (e.g., Ménégoz et al., 2018; Robock & Liu, 1994; Yang et al., 2019) due to differences in model parameterizations, representations of the forcing, initialization, and volcanic parameters.

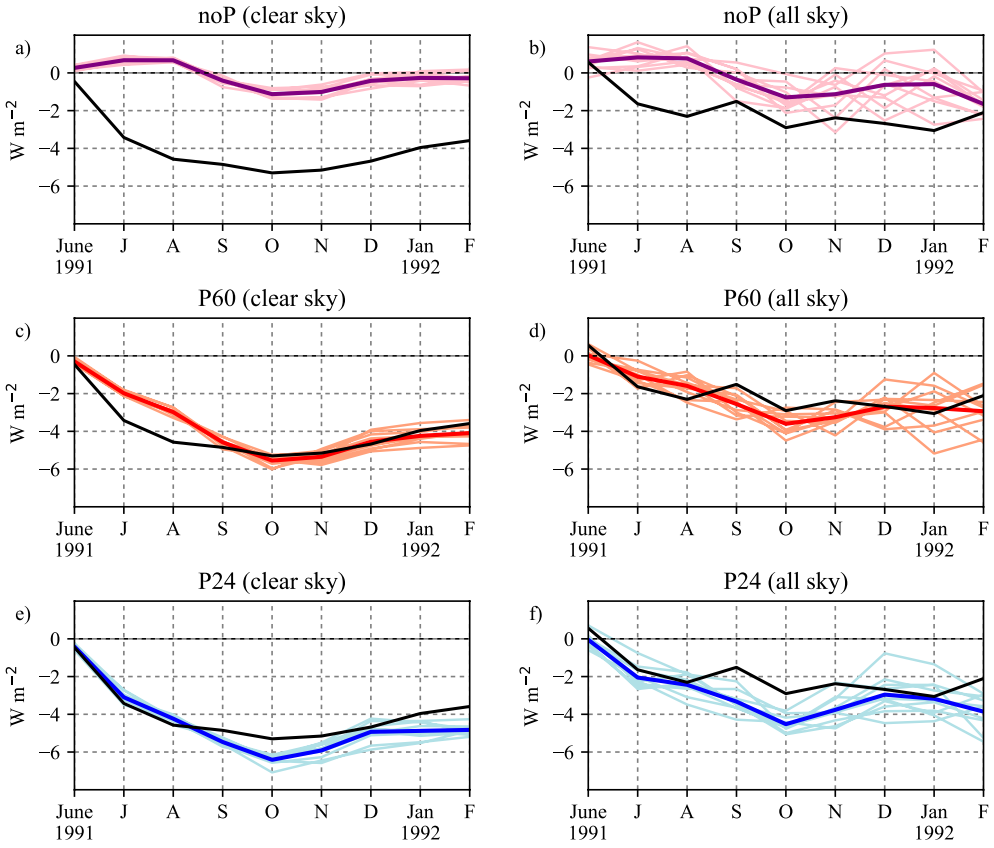

Figure 1. Global mean net shortwave radiation at the surface in MERRA-2 (black lines) and in the GEOS-S2S forecasts. Forecasts are calibrated with respect to the drift (see text for details). MERRA-2 anomalies are calculated with respect to the 1981–2011 climatology. Thick lines show the ensemble means, while thin lines show each ensemble member.

Several observational and modeling studies have found a decrease in global mean precipitation after large volcanic eruptions (e.g., Gu & Adler, 2011; Gu et al., 2007; Iles et al., 2013; Robock & Liu, 1994; Trenberth & Dai, 2007). In particular, Joseph and Zeng (2011) performed coupled model simulations of post-Agung, post-El Chichón, and post-Pinatubo periods to find that the decrease in tropical precipitation over land is associated with a weaker monsoonal circulation due to a suppressed land-sea temperature contrast.

The role that the eruption played in the development of the strong 1991–1992 El Niño is less certain. When Mt. Pinatubo erupted, sea surface temperatures (SSTs) in the central Pacific Ocean were already warmer than average. The Niño 3.4 index (the SST anomaly from the 30-year climatological mean between ±5° latitude and 170°–120°W longitude) exceeded 0.4°C the month prior the eruption, marking the start of an El Niño event. It remained above this threshold until June 1992 after peaking in January 1992. Several studies have suggested a connection between tropical volcanic eruptions and the El Niño Southern Oscillation (ENSO; McGregor et al., 2020). Paleoclimate (Adams et al., 2003; McGregor et al., 2010) and modeling (e.g., Clement et al., 1996; Emile-Geay et al., 2008; Lim et al., 2016; Mann et al., 2005; Ohba et al., 2013; Predybaylo et al., 2017; Stevenson et al., 2016; Zuo et al., 2018) studies concluded that a volcanic forcing drives the Pacific Ocean toward conditions that favor the strengthening of El Niño in the year of the eruption. Clement et al. (1996) found, using an idealized coupled ocean-atmosphere dynamical model (Zebiack & Cane, 1987), that western Pacific SSTs are mainly regulated by a one-dimensional energy balance, while changes in eastern Pacific SSTs are partially balanced by changes in ocean advection. This results in a zonally non-uniform temperature response across the Pacific Ocean, where the western Pacific responds faster to a forcing than the eastern Pacific. In the case of the negative forcing from Mt. Pinatubo, this "ocean dynamical thermostat" (ODT) results in a flattening of the zonal temperature gradient and a subsequent weakening of the trade

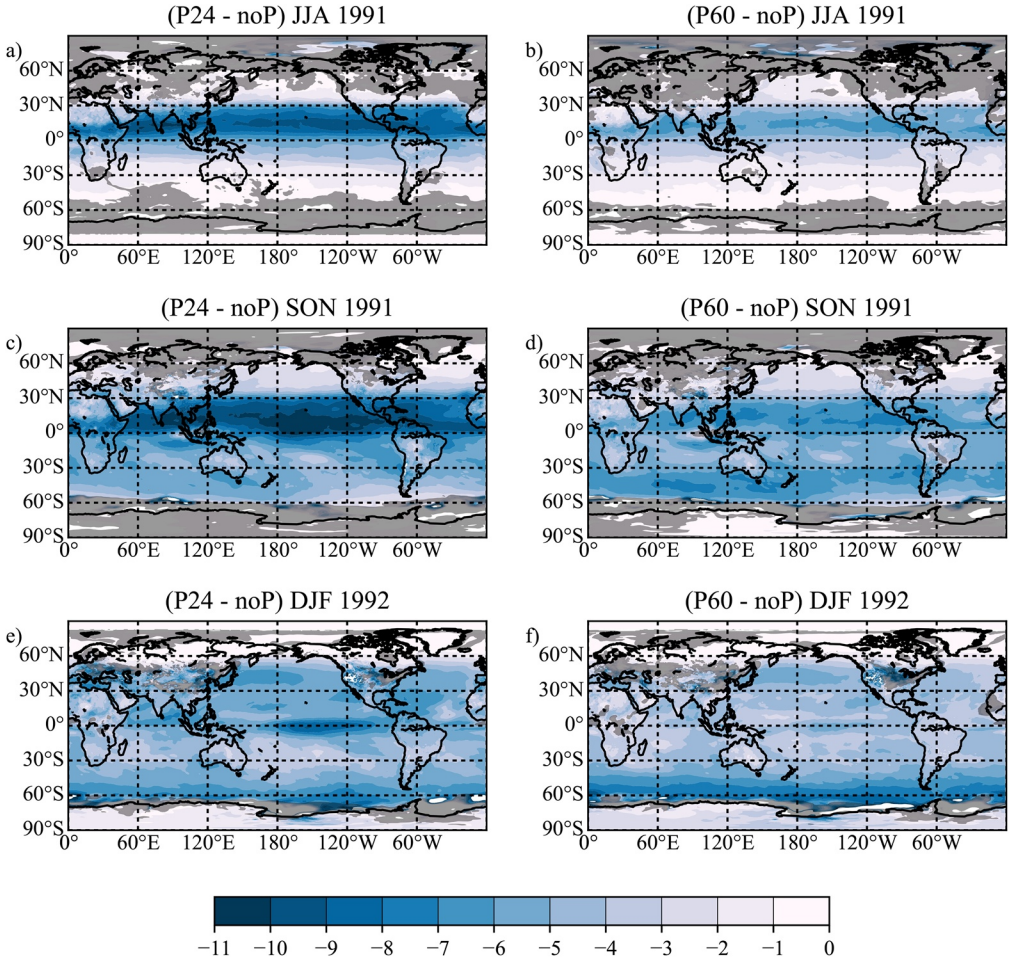

Figure 2. Seasonal maps of the decrease in clear sky shortwave radiation (W/m^2) due to the volcanic aerosol from Mt. Pinatubo, calculated as the difference between the forecasts with and without the eruption. Areas not significant at 95% level are shaded in gray.

winds (Bjerknes, 1969), creating conditions favorable to the development of El Niño. More recently, studies using fully coupled climate models found that the weakening of the trade winds after a volcanic eruption is caused by volcanic changes other than the ODT mechanism, such as a cooling of the Maritime Continent that weakens the Walker circulation (Ohba et al., 2013), a shift in the ITCZ caused by the cooling of the tropical Pacific (Lim et al., 2016) or by the differential cooling between hemispheres (Pausata et al., 2020; Schneider et al., 2009), or a cooling of tropical Africa that suppressed precipitation and altered the Walker circulation through anomalous Kelvin waves (Khodri et al., 2017). Pausata et al. (2020) also found that extratropical teleconnections associated with the volcanic change in meridional temperature gradient and land-ocean temperature contrast weaken the Pacific subtropical high-pressure system and cause a westerly wind anomaly in the equatorial Pacific.

Other studies suggested that tropical volcanic eruptions favor the development of La Niña. McGregor and Timmermann (2011) found that Newtonian cooling and changes in mixed layer depth offset the warming caused by the ODT and the other mechanisms mentioned above. Wang et al. (2018) found that strong tropical volcanic eruptions are generally followed by La Niña cooling that persists from the eruption to about 5 months after the peak in volcanic forcing. They attribute this response to the quick cooling of the western coast of South America, which strengthens the trade winds, but also recognize that this did not happen after Pinatubo possibly because of the weakness of the cooling of the eastern equatorial Pacific and the state of the tropical Pacific at the moment of the eruption. Generally, Meehl et al. (2015) found that CMIP5

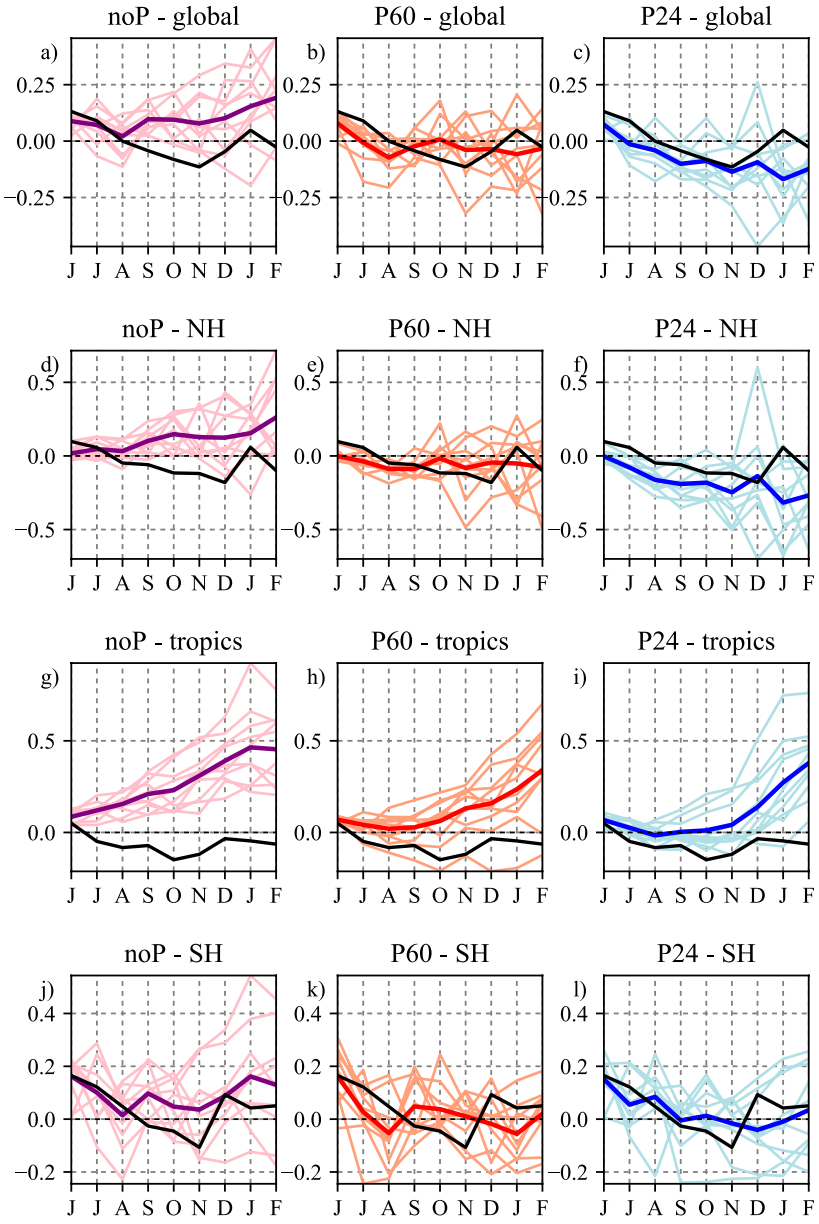

Figure 3. Surface temperature anomaly in MERRA-2 (black lines) and in the GEOS-S2S forecasts. From top to bottom, the panels show global, northern hemispheric, tropical (20°S–20°N), and southern hemispheric means. Forecasts are calibrated with respect to the model drift and MERRA-2 anomalies are calculated with respect to the 1980–2010 climatology. Thick lines show the ensemble means, while thin lines show each ensemble member.

models on average simulate a cooling of the tropical Pacific in the first winter after the Pinatubo eruption. Khodri et al. (2017), however, showed that also CMIP5 models develop El Niño after large tropical volcanic eruptions when considering SST anomalies relative to the tropical average, effectively removing the global cooling effect of the volcanic aerosol.

The goal of this study is to establish the validity of seasonal forecasts in the event of a volcanic eruption taking place after the forecasts have been produced. Despite representing a major perturbation of the climate system, volcanic eruptions are generally not included in seasonal forecasting systems for mainly two reasons. First, such eruptions are rare and generally not predictable. Second, the model systems used for seasonal forecasting typically do not contain the aerosol mechanisms needed to compute the aerosol impacts, but rather include the average radiative effect of aerosols using climatologies (Benedetti & Vitart, 2018).

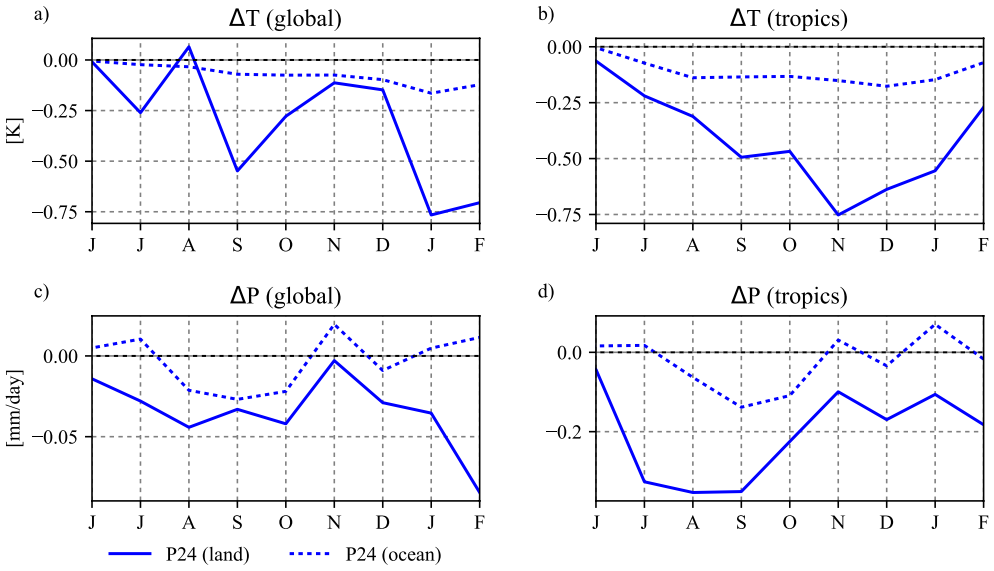

Figure 4. Impact of the volcanic aerosol on global and tropical (20°S–20°N) mean surface temperatures (above) and precipitation (below), calculated as the difference between P24 and noP. Each panel shows the average over land (solid) and ocean (dashed).

Specifically, in this study we investigate whether the inclusion of the 1991 eruption of Mt. Pinatubo would have significantly changed seasonal predictions of surface temperatures, ENSO development, and precipitation in the NASA Goddard Earth Observing System Seasonal to Subseasonal forecasting System (GEOS-S2S), which is used to produce forecasts up to 9 months into the future.

GEOS-S2S (Molod et al., 2020) is an optimal system for this study because it prognostically simulates aerosol concentrations and includes their radiative interaction as well as their indirect effect on clouds. Volcanic forcing is calculated based on a prescribed injection of SO_2, rather than using prescribed climatologies of stratospheric aerosol optical thickness. As such, the spread of the GEOS-S2S ensemble members represents the uncertainty in forecasted forcing arising from the natural variability in the transport of the volcanic aerosol.

This paper is organized as follows: Section 2 presents a description of the GEOS-S2S system in the operational forecast setup; Section 3 reports the results of the simulations in terms of radiative forcing and subsequent response in surface temperatures, ENSO development, and precipitation; Section 4 summarizes and discusses the results.

2. Model Description and Simulations

This study employs forecasts produced with Version 2 of the GEOS-S2S system, described in detail by Molod et al. (2020). This system is used each month to compute nine-month seasonal forecasts that are distributed broadly, including to the North American Multi-Model Ensemble (Kirtman et al., 2014), through the NASA Goddard Modeling Assimilation Office (GMAO) website. The atmospheric model includes the dynamical core of Putman and Lin (2007). The physical parameterizations are updated from the version described by Molod et al. (2015) in several ways. The key update is the inclusion of the two-moment cloud microphysics code (Barahona et al., 2014) that allows for indirect aerosol-cloud interactions (as well as the direct effects, which were already included in Version 1). GEOS-S2S couples the atmospheric model to the Modular Ocean Model, Version 5 (MOM5) (Griffies, 2012; Griffies et al., 2005), the Catchment model (Koster et al., 2000), and the Sea Ice Model (CICE) (Hunke & Lipscomb, 2010).

For this study, the most relevant feature of the GEOS-S2S system is that it includes the Goddard Chemistry Aerosol Radiation and Transport (GOCART, Colarco et al., 2010; Randles et al., 2017) aerosol module,

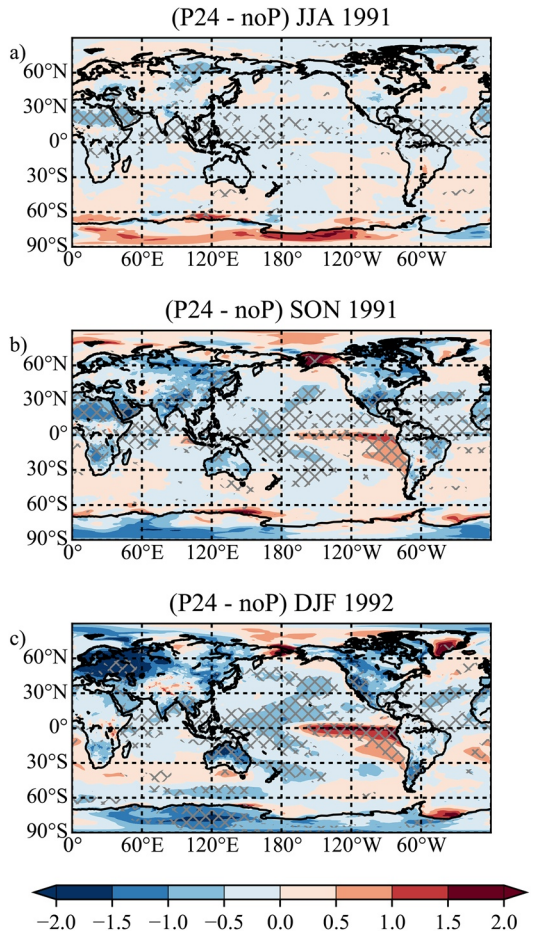

Figure 5. Impact of the volcanic aerosol on seasonal surface temperatures (in K), calculated as the difference between P24 and noP. Hashed areas are significant at 95% level.

with representations of dust, sea salt, organic and black carbon, and sulfate aerosol. The use of prognostic aerosol distributions in GEOS-S2S enables studies of aerosol impacts on the climate and its variability on seasonal time scales, in a similar manner to the European Centre for Medium-Range Weather Forecasts (ECMWF) Integrated Forecasting System (IFS) experimental configuration used in Benedetti and Vitart (2018). GOCART simulates aerosols with a bulk approach, which means that aerosol size distributions are prescribed *apriori* based on observations. GEOS-S2S/GOCART routinely assumes that the size distribution of sulfate aerosols follows a lognormal distribution with modal radius 0.0695 μm and standard deviation 2.03 (corresponding to an effective radius equal to 0.24 μm). This distribution is appropriate for tropospheric aerosol, but observations of the post-Pinatubo period measured a larger radius for the volcanic aerosol (Bingen et al., 2004a, 2004b). Accordingly, the GOCART module has been extended after Aquila et al. (2016) to include an additional sulfate aerosol tracer in the stratosphere with modal radius 0.35 μm and standard deviation 1.59 (effective radius = 0.6 μm), which is in the range derived from SAGE II observations during the post-Pinatubo period.

In GEOS, volcanic eruptions are simulated as an injection of SO_2 in the model grid boxes directly above the volcano. The SO_2 is uniformly distributed vertically between altitudes specified for each eruption. The conversion of SO_2 into sulfate aerosols is then calculated online using climatological ozone and OH distributions. In our simulations, the 1991 eruption of Mt. Pinatubo is represented as a set of three eruptions on June 13, 14, and 15, respectively. The June 13 eruption was included as a 0.14 Tg SO_2 injection in the 13–19 km layer and the June 14 eruption as a 0.054 Tg injection in the 17–25 km layer, following the database by Carn et al. (2015) and subsequent updates. The climactic eruption of June 15 was simulated as an injection of 16 Tg SO_2 in the 18–22 km layer. The altitude of the June 15 injection is lower than Carn et al. (2015) to achieve a better agreement of the GEOS simulations with observations (Aquila et al., 2012).

Three ensembles of 9-month predictions were carried out:

1. *NoP* does not include the eruption of Mt. Pinatubo (the standard configuration of GEOS-S2S near-real time forecasts).
2. *P24* includes the eruption of Mt. Pinatubo with a sulfate aerosol effective radius of 0.24 μm (same as tropospheric sulfate).
3. *P60* includes the eruption of Mt. Pinatubo with a sulfate aerosol effective radius of 0.6 μm.

All simulations were run with a horizontal resolution of about 0.5° by 0.5° longitude by latitude in the atmosphere and ocean component. The atmospheric component uses 72 vertical hybrid levels up to 1 Pa, while the ocean component uses 40 layers down to a depth of 4,500 m. Each monthly ensemble of forecasts consists of 10 simulations initialized with a "lagged-burst" strategy, for which four simulations are initialized on May 16, 21, 26, and 31, 1991 and the remaining six on May 31 using initial conditions obtained by perturbing 3-D variables in the ocean and atmospheric components, as documented in Molod et al. (2020) and Schubert et al. (2019). These perturbations are intended to represent the uncertainty in initial conditions and provide a means of generating spread in the 10-member ensemble of monthly forecasts. Importantly, since the spatial distribution of the volcanic aerosol is determined by the transport of SO_2 and sulfate aerosols, the spatio-temporal distribution of the volcanic forcing differs among ensemble members. We are aware of the statistical limitations associated with an ensemble of only 10 members, but, as the goal of this study is to quantify the validity of the GEOS-S2S seasonal forecasts in case of the volcanic eruption, it is important that we maintain the same setup as the operational forecast system. At the moment, the delivery

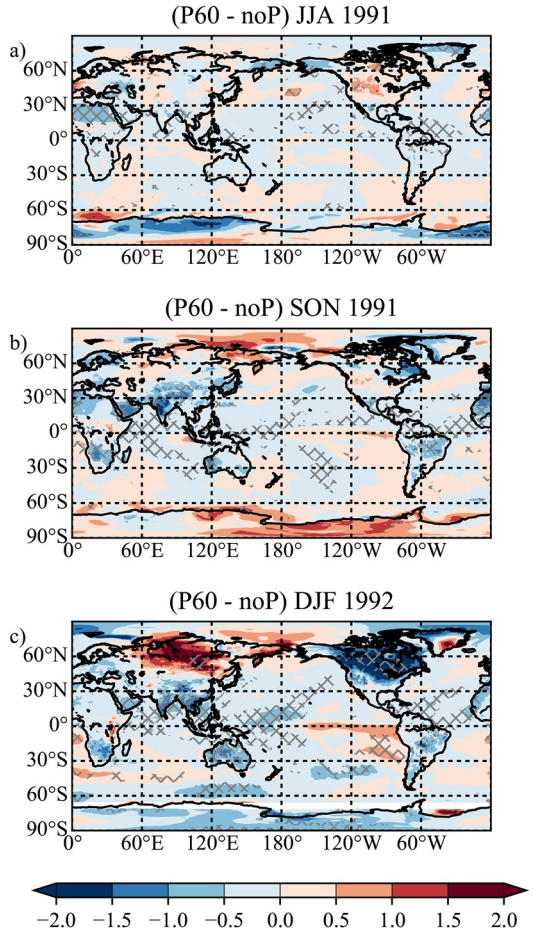

Figure 6. As Figure 5 but for P60.

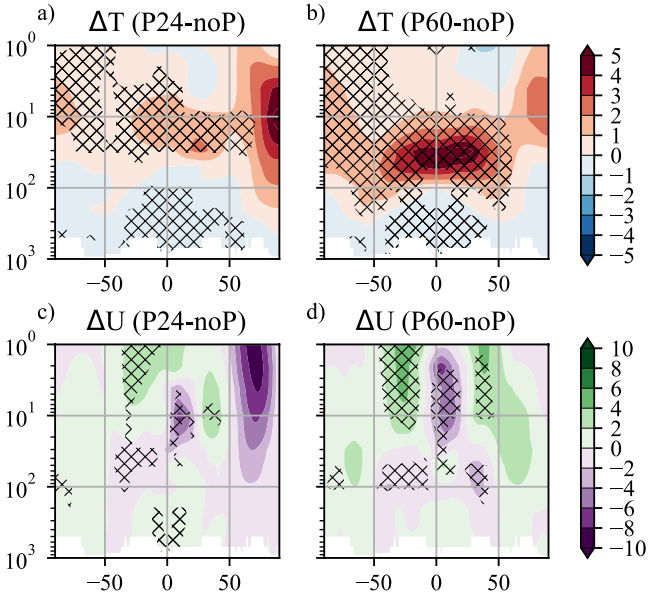

Figure 7. Vertical profile of the zonal mean temperature (a and b, in K) and zonal winds (c and d, in m/s) anomalies in P24 (left panels) and P60 (right panels). Hatched areas are statistically significant at 95% level.

constraints of a seasonal forecast model with prognostic aerosol do not allow for larger ensembles to be run routinely with GEOS-S2S. Indeed, the choice of 10 ensemble members is common among such operational models (see Table 2 in Kirtman et al., 2014).

In the following, results from the forecast simulations are all calibrated with respect to the single model drift, which is defined as the average of all forecasts initialized on the same day (May 15, 21, 26, and 31 for our study) of each year from 1981 to 2010. This calibration follows the convention by Stockdale (1997) to eliminate any long-term climate bias arising from an imperfectly simulated energy flux balance. For comparison, we also show temperature and precipitation anomalies from MERRA-2 (Gelaro et al., 2017). For consistency with the drift, MERRA-2 anomalies are calculated with respect to the May 1981–April 2011 monthly climatological means. To isolate the effect of the eruption on the forecasts, we also show the difference between the ensembles with and without Pinatubo, calculated by pairing simulations initialized with the same sets of initial conditions. The statistical significance of the difference between P24 or P60 and noP is calculated with a paired Student's *t*-test at 95% significance level.

3. Results

3.1. Radiative Forcing

The direct impact of the volcanic sulfate aerosols is to scatter visible radiation and reduce the shortwave radiation reaching the surface (Figure 1). The inclusion of the volcanic eruption in the forecast simulations brings the reduction in surface SW radiation in good agreement with MERRA-2 when calculated over clear and all sky. Smaller aerosols scatter shortwave radiation more efficiently than larger ones, and as a consequence less radiation reaches the surface in P24 than in P60. While P24 is closer to MERRA-2 than P60 during the first 3 months after the eruption, P60 provide a better agreement afterward. This is due to the fact that the aerosol module used in GEOS-S2S does not simulate the evolution of the aerosol size distribution, while, in reality, the effective radius of the volcanic aerosols grows over time from about 0.2 μm shortly after the eruption to about 0.6 μm 6 months after the eruption (e.g., Figure 1 of English et al., 2013). This makes the aerosol optical properties assumed in P24 more appropriate for the first half of the simulations, and the ones of P60 afterward.

The latitudinal pattern of the radiative forcing is overall similar in P60 and P24 (Figure 2): the forcing is generally zonally uniform and mostly confined within the tropics until August 1991. As expected, the magnitude of the forcing is larger in P24, with the peak forcing over the central Pacific reaching −11 W/m^2 in P24 and only −7 W/m^2 in P60.

3.2. Surface Temperature

The inclusion of the Pinatubo aerosols improves the forecast of global and hemispheric mean surface temperatures (Figure 3). The standard forecast, which excludes the impacts of the eruption, is warmer than MERRA-2 in at all latitudes, particularly in the tropics (Figure 3g). The inclusion of the volcanic aerosol cools surface temperatures in both

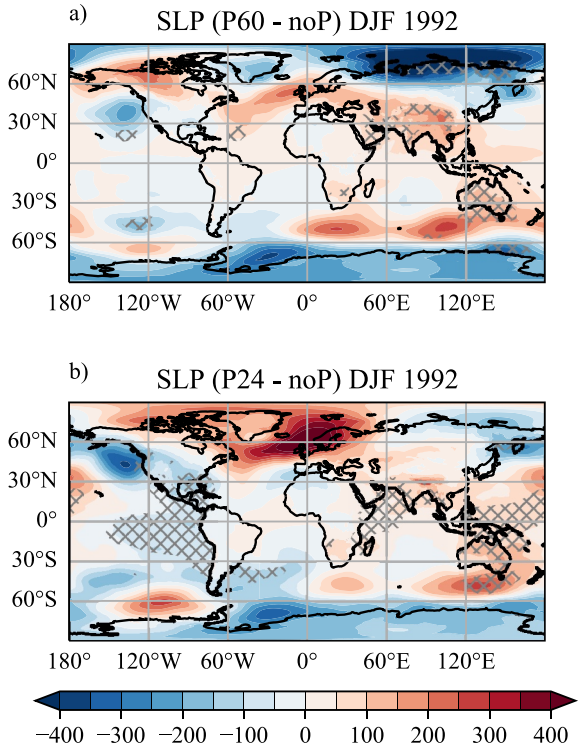

Figure 8. Sea level pressure anomalies (in Pa) averaged in the first winter after the eruption in P60 (a) and P24 (b). Hatched areas are statistically significant at 95% level.

hemispheres and in the tropics, while still overestimating the warming of the tropics with respect to MERRA-2. The response to the volcanic forcing is faster and stronger in the northern hemisphere because of the lower heat capacity of land masses.

The volcanic cooling is more than three times stronger over land than over ocean, both in the global mean and over the tropics (Figures 4a and 4b). Globally, the largest cooling is achieved in January over land and over ocean. In the tropics, the volcanic cooling peaks in November and then diminishes due to the decrease in volcanic forcing (Figure 2) and the strengthening of El Niño (Section 3.3). P60 shows a similar response (Figure S1). The spatial pattern of the temperature response to the eruption is similar in the two forecast experiments (Figures 5 and 6), with a cooling of the land masses and a strengthening of El Niño, but the significant areas are much smaller in P60 than in P24. Regionally, the response to the volcanic forcing does not necessarily scale with the forcing itself. While the simulated volcanic cooling over Europe is stronger in P24 than in P60, the contrary is true for North America despite the smaller forcing in P60. This could be due to the indirect effects of a stronger El Niño in P24 than in P60 (Section 3.3). The noP ensemble, which develops a strong El Niño but does not include the volcanic eruption, forecasts a significant surface warming of North America (Figure S2), suggesting that the forecasted El Niño creates warm conditions in north America (Halpert & Ropelewski, 1992) that offset part of the volcanically induced cooling in P24.

P60 simulates a winter warming over northern Asia (Figure 6e), which is not present in P24 (Figure 5e). Previous studies have found that tropical volcanic eruptions can cause a winter warming over northern hemispheric land masses through a stratospheric pathway (Graf et al., 1993) initiated by the stratospheric warming associated with the sulfate aerosols absorption of infrared and near-IR radiation. This stratospheric warming increases the latitudinal temperature gradient and leads to a stronger polar vortex, which causes a positive phase of the North Atlantic Oscillation and subsequent warmer weather over Asia. In our simulations, the forecasted stratospheric warming is stronger in P60 than in P24 (Figures 7a and 7b), because larger particles absorb more strongly infrared radiation than smaller particles (while scattering less efficiently in the visible). As such, P60 causes a significant strengthening of the polar vortex that is absent in P24 (Figures 7c and 7d). As in Graf et al. (1993), this results in an increase in the north-Atlantic sea level pressure gradient in P60 (Figure 8), which, however, is not statistically significant. It is important to notice that the temperature anomaly and the area experiencing significant warming are small, and that the westerly wind change at 60°N and 10 hPa, which is often used as a measure of polar vortex strength, is less than 4 m s^{-1} and not statistically significant

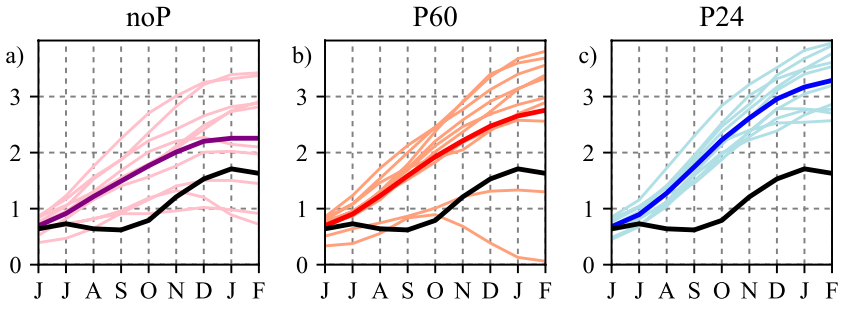

Figure 9. Evolution of the ONI index in NOAA-CPC data set (black lines) and in the GEOS-S2S forecasts. The ONI index is defined as the three-month running mean sea surface temperature anomaly in the Niño 3.4 region (5°S–5°N; 120–170°W). Forecast anomalies are calculated with respect to the drift. Thick lines show the ensemble means, while thin lines show each ensemble member.

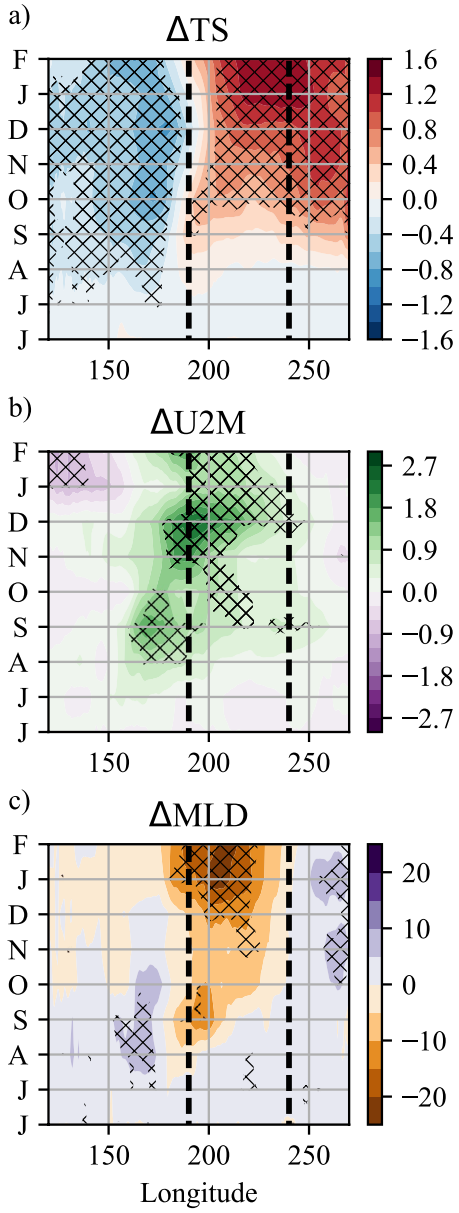

Figure 10. Hovmöller diagram of the impact of the volcanic aerosol in the tropical Pacific (5°S–5°N) on (a) surface temperature (K), (b) 2-m zonal wind (m/s) with green (positive) indicating westerly anomalies, and (c) mixed layer depth [m] with blue (positive) indicate a deepening of the mixed layer. The volcanic impact is calculated by subtracting noP from P24. Hatches mark regions that are significant at 95% level. Dashed lines mark the longitudinal boundaries of the Niño 3.4 box.

(Figure 7d), as found by Polvani et al. (2019). A larger ensemble is needed to verify whether the Asian winter warming is a robust response. We include in the supporting information the forecasted temperatures for Europe, northern Asia, northern Africa, and North America (Figure S3).

3.3. ENSO Development

In all three forecast experiments, even without the inclusion of the eruption, SSTs in the equatorial Pacific Ocean develop an El Niño that is longer and more intense than the observations (Figure 9). The introduction of the volcanic forcing reduces the ensemble spread, particularly in P24 (Figure 9c) because the strong volcanic forcing dominates over the variability introduced by the uncertainty over the initial conditions. We focus in this section on P24, as it shows a clearer response in ENSO. Results for P60 (Figures S4 and S5) show that the changes leading to the ENSO development are similar to P24, but the difference between P60 and noP is not statistically significant at the 95% level.

Despite the fact that the volcanic forcing is zonally uniform (Figure 2c), the temperature response associated to such forcing is a cooling in the western Pacific and a later warming in the central and eastern Pacific (Figure 10a). GEOS-S2S predicts a weakening of the trade winds (westerly anomalies in Figure 10b) that further weakens the SST gradient via the Bjerknes feedback and leads to a deeper mixed layer in the eastern Pacific (Figure 10c), promoting conditions favorable to the development of El Niño.

As in Predybaylo et al. (2017), we calculate the terms in the equation for the mixed layer temperature from Stevenson and Niiler (1983) and Huang et al. (2010) (Figure 11):

$$\frac{dT_{ML}}{dt} = -w_H \frac{T_{ML} - T_H}{H} - u_{ML} \frac{\partial T_{MLA}}{\partial x} - v_{ML} \frac{\partial T_{ML}}{\partial y} + \frac{Q_{net}}{\rho C_p H} + Q_{res},$$

where T is the ocean temperature, u, v and w the zonal, meridional, and vertical components of the ocean currents, Q_{net} the net surface energy flux, ρ the density of seawater (1,029 kg m^{-3}), C_p the specific heat capacity of seawater at constant pressure (3,990 J kg^{-1} K^{-1}), Q_{res} the residual, and H the mixed layer depth. The mixed layer depth is defined following Sprintall and Tomczak (1992) as the depth at which the potential density is equal to the surface potential density plus the density change needed to reach a temperature difference from the surface equal to 0.5°C keeping salinity constant. The indices ML and H indicate that a variable is averaged across the mixed layer or is sampled at the model level below the mixed layer, respectively. In the first three months after the eruption (JJA), the only significant change due to the volcanic aerosol is the radiative cooling from the reduction in surface energy flux. During the following three months (SON) the decrease in surface heat flux keeps driving the cooling of the central Pacific (Niño 4), while the surface sea temperature in the eastern Pacific (Niño 3) increases due to the weakening of the easterly winds, reflected in the warming associated to zonal advection term, as well as the suppression of vertical upwelling, reflected in the vertical advection term. Between December 1991 and February 1992, the eruption causes a warming in both regions due to changes in horizontal advection in the central Pacific and to zonal and vertical in the eastern Pacific.

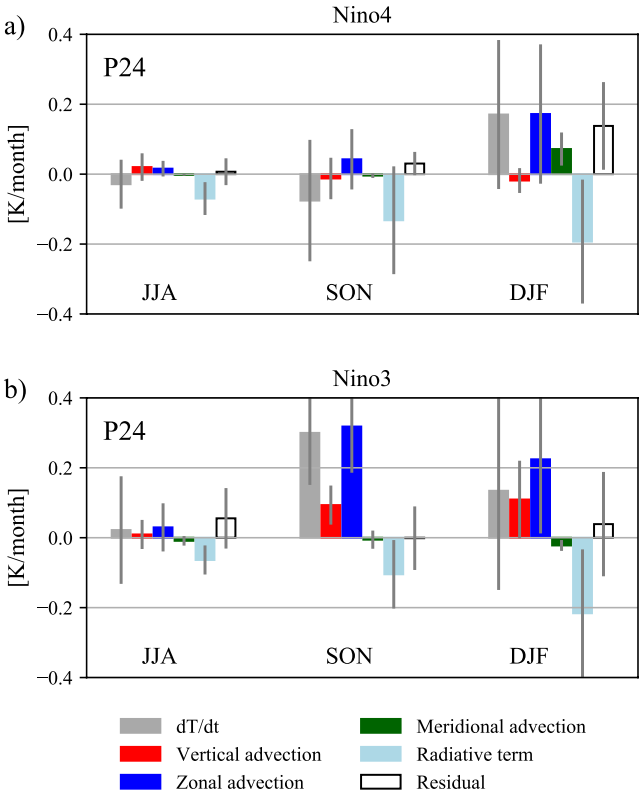

Figure 11. Changes in the terms of the mixed layer energy budget caused by Mt. Pinatubo in the (a) Niño 4 (5°S–5°N, 160°E–150°W) and (b) Niño 3 (5°S–5°N, 150°W–90°W) boxes, seasonally averaged from June 1991 to February 1992. The changes are calculated as the difference between P24 and noP. The error bars indicate one standard deviation.

3.4. Precipitation

Generally, the inclusion of the volcanic aerosol improves the skills of the forecast with respect to precipitation (Figure 12). At the beginning of the simulation, the forecasted precipitation anomaly over the northern hemisphere is biased high with respect to MERRA-2. The inclusion of the volcanic aerosols causes a decrease in precipitation in the northern hemisphere (Figures 12d–12f) and an increase in the southern hemisphere (Figures 12j–12l), improving the agreement with MERRA-2. This is consistent with the southward shift of the ITCZ shown in Figure 13. Schneider et al. (2009) attributed the shift of the ITCZ after a tropical volcanic eruption to the fact that, even with a latitudinally symmetric distribution of aerosol, the volcanic cooling is stronger in the summer than in the winter hemisphere and, as such, the seasonal migration of the ITCZ extends less into the summer hemisphere. Additionally, the norther hemisphere reacts more strongly to a forcing than the southern hemisphere due to the larger land masses.

The volcanic forcing decreases precipitation more strongly over land than over ocean (Figures 4c and 4d). In the tropics, the decrease in precipitation anticipates the decrease in temperature by about 3 months (Figures 4b and 4d). Over land in the tropics, the volcanic impact on temperature reaches its maximum in November (−0.25%) and on precipitation in September 1991 (−7.8%), one month after and one before the peak in volcanic forcing (Figure 1), respectively. Gu and Adler (2011) also found that the precipitation response anticipates the peak in volcanic forcing as well as the temperature response to the eruption.

P24 and P60 show a similar pattern of precipitation changes, with larger significant areas in P24 (Figures 13 and 14). GEOS forecasts a statistically significant drying of northern tropical Africa and China from June to November 1991. There are no other statistically significant precipitation changes over land in the 9-month forecast. GEOS forecasts a clear southward shift of the ITCZ, which becomes significant starting from September to November 1991.

4. Summary and Conclusions

The aim of this study was to identify whether the inclusion of the 1991 eruption of Mt. Pinatubo introduces significant changes in seasonal forecasts produced with the near-real time NASA GEOS-S2S prediction system. We performed one control forecast without volcanic eruption, which represent the standard forecast produced by GMAO, and two sensitivity experiments varying the assumptions on the radius of the volcanic sulfate aerosols. Smaller aerosol particles decrease the net surface shortwave radiation more than larger particles, due to the higher aerosol scattering efficiency in the visible range. They, however, produce a smaller stratospheric warming because they absorb infrared and near-infrared radiation less efficiently than larger particles.

We find that the inclusion of the volcanic aerosol improves the skills of the forecasts with respect to the global and hemispheric surface mean temperatures and precipitation. The volcanic radiative forcing produces a cooling of the forecasted global mean temperature and a reduction in precipitation, in agreement with previous studies (e.g., Broccoli et al., 2003; Gu et al., 2007; Iles et al., 2013; Joseph & Zeng, 2011; Meyer et al., 2016; Robock & Liu, 1994; Schneider et al., 2009). The regional temperature response is not always proportional to the forcing. For instance, the cooling over north America is stronger in P60 than in P24, despite the smaller radiative forcing. This could be due to a combination of the direct effect of the reduction in surface shortwave radiation with the indirect effects on surface climate caused by El Niño. A warming over northern Asia in the winter following the eruption, as found by Graf et al. (1993) and Robock and Mao (1992), is forecasted in P60 and not in P24, possibly because P60 shows a stronger stratospheric

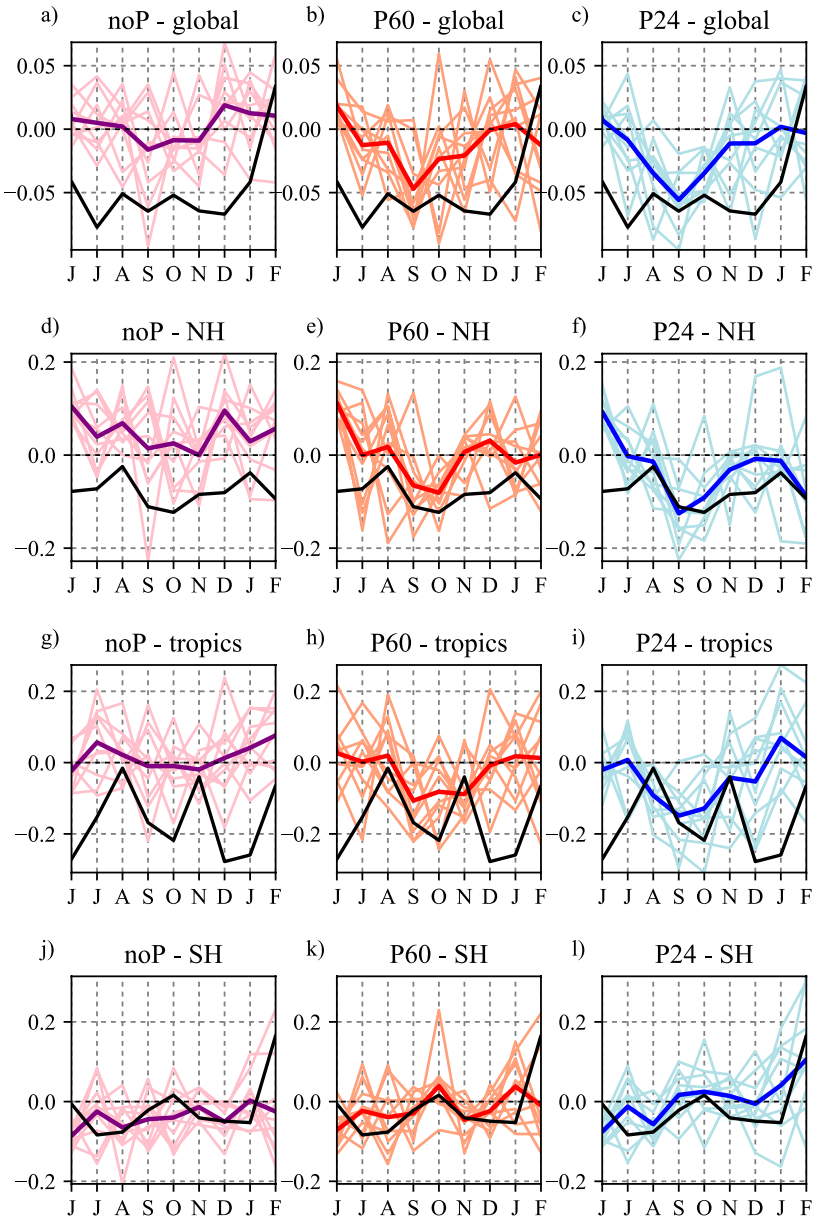

Figure 12. Precipitation anomaly in MERRA-2 (black lines) and in the GEOS-S2S forecasts. From top to bottom, the panels show global, northern hemispheric, tropical (20°S–20°N), and southern hemispheric means. As in Figure 1, forecasts are calibrated with respect to the drift and MERRA-2 anomalies are calculated with respect to the 1981–2011 climatology. Thick lines show the ensemble means, while thin lines show each ensemble member.

warming and strengthening of the polar vortex. The changes in the polar vortex, however, are very small when compared to the wind speed characteristics of the vortex. We cannot therefore be confident that these regional signals would still hold in a larger ensemble, especially in regions characterized by large variability.

The inclusion of the Pinatubo eruption decreases the forecast skills in the tropical Pacific. The volcanic forcing strengthens the forecasted El Niño, which was overestimated even in the forecast without volcanic eruption. The analysis of the mixed layer energy budget indicates that the warming of the tropical Pacific is caused by changes in horizontal and vertical advection that offset the cooling associated with the decrease in net surface shortwave radiation. Our results agree with previous studies that found that volcanic eruptions favor the development of El Niño. GEOS-S2S forecasts a cooling and drying of tropical Africa (Khodri et al., 2017), a southward shift of the ITCZ (Lim et al., 2016; Pausata et al., 2020; Schneider et al., 2009), and

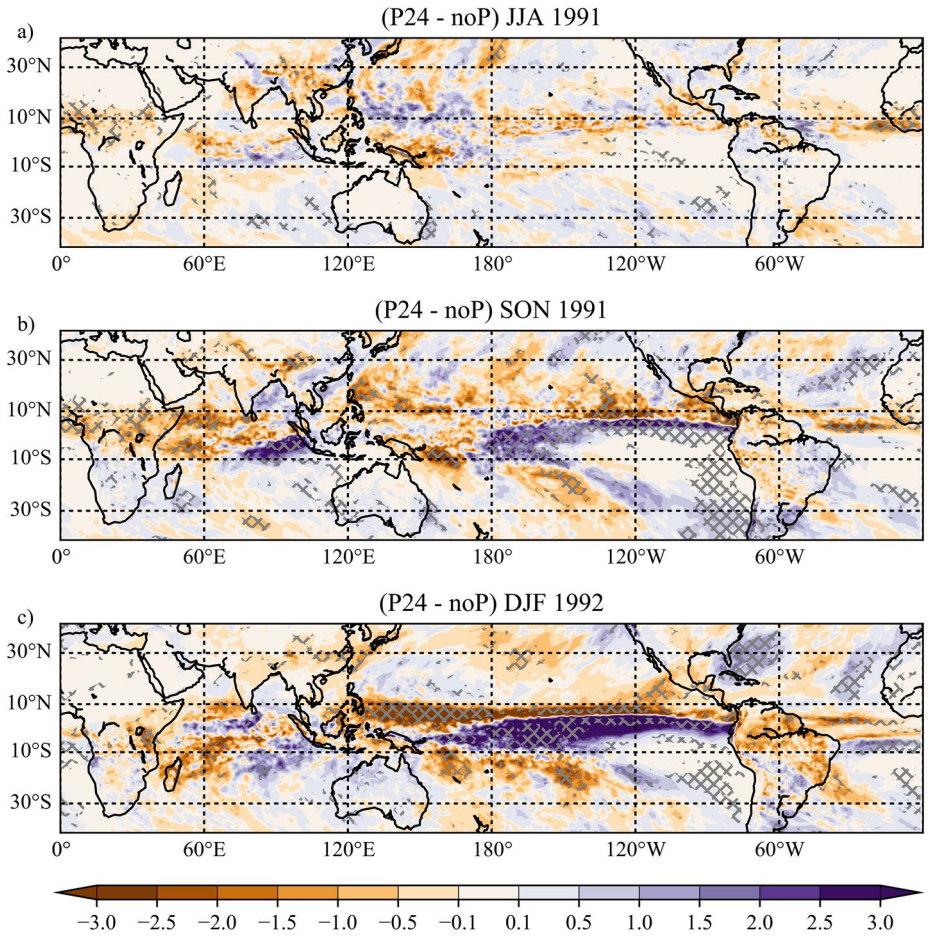

Figure 13. Impact of the volcanic aerosol on precipitation (in mm/day), calculated as the difference between P24 and noP. Hashed areas are significant at 95% level. Corresponding global maps, as well as the absolute values of precipitation rates, are included in Figures S6 and S8.

a cooling of the Maritime Continent (Ohba et al., 2013). All of these changes have been identified by the studies above cited as driving the equatorial Pacific Ocean into an El Niño state. Sensitivity tests that isolate each mechanism are needed to identify which one is the main driver of the development of El Niño. As we focus here on the validity of the GEOS-S2S forecast in the event of a volcanic eruptions, such sensitivity tests are beyond the scope of this study. In the same way, we are unable to determine to which extent initial conditions impact the volcanic response (Predybaylo et al., 2017), since we performed experiments starting from the actual state of the Pacific at the time of the eruption, as we would do if we were to newly produce forecasts in case of an eruption.

Our results do not agree with McGregor and Timmermann (2011) and Wang et al. (2018), who found that volcanic eruptions move the Pacific into La Niña state at the peak of the volcanic forcing. However, McGregor and Timmermann (2011) considered volcanic eruptions that produced a maximum global mean effective radiative forcing of -4 W/m^2, larger than the one simulated by GEOS-S2S for Pinatubo, and Wang et al. (2018) noted that the fact that El Niño was already underway at the moment of the Pinatubo eruption could be the reason why La Niña was not observed after the eruption. With our current set of simulations, we are unable to say whether with a stronger volcanic forcing Newtonian cooling would overwhelm any impact due to changes in advection.

These results show that the inclusion of eruptions of magnitude up to Mt. Pinatubo produces statistically significant changes mainly at tropical latitudes in the GEOS-S2S seasonal forecast system. While some significant changes are produced also in mid- and high-latitude temperature fields, the same is not true

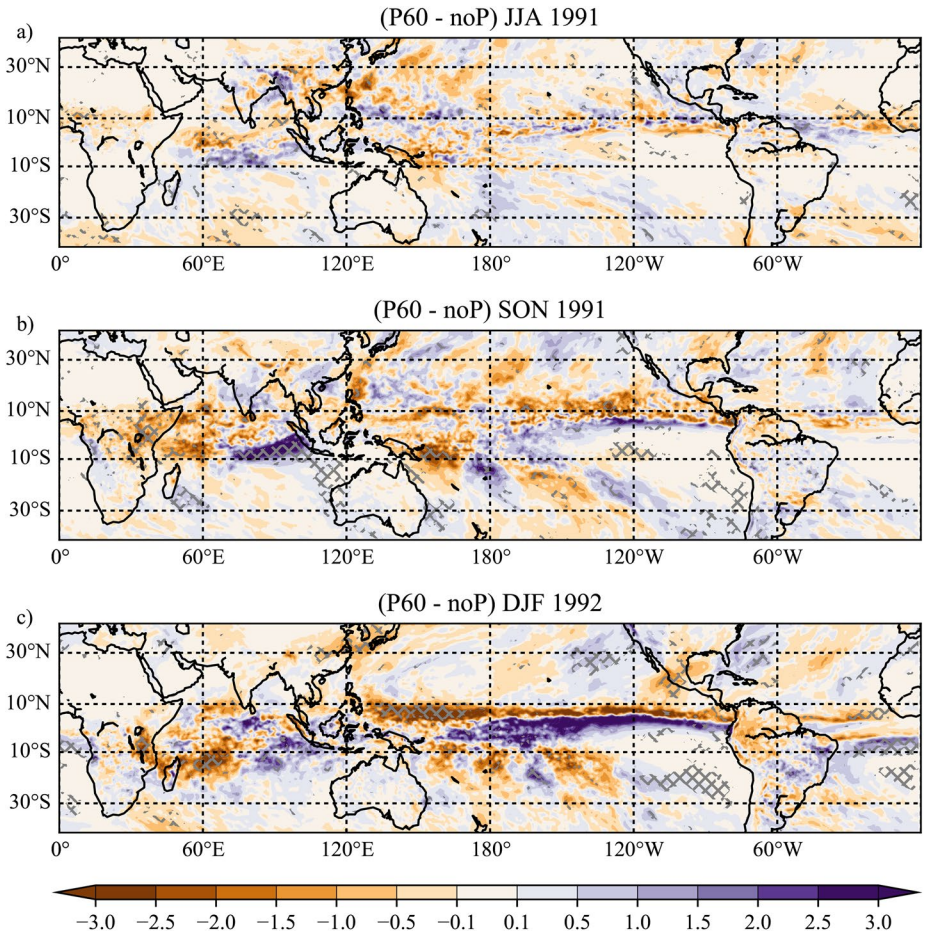

Figure 14. As Figure 13 but for P60. Corresponding global maps are included in Figure S7.

for precipitation, especially over land, at least with the current 10-member ensemble configuration. This means that the additional cost of producing new forecasts in the event of a large eruption would not uniformly modify the predictions at a regional level. The results presented herein do not preclude significant impacts of much larger eruptions, nor does it guide decisions on model configurations on the substantial ash loading in the troposphere that arise from volcanic eruptions, where the impacts occur on much shorter timescales and provide direct hazards for human health, the environment, and aviation safety.

Finally, although any seasonal prediction system cannot predict an explosive eruption beforehand, the NASA Global Modeling Assimilation Office (GMAO) plants on re-running GEOS-S2S seasonal predictions in case such an eruption should occur. The use of the GOCART interactive aerosol and the inclusion in the model physics of the aerosol indirect effect, not included in any other near real-time seasonal prediction systems, makes GEOS-S2S uniquely suited to studies of the impact of explosive eruptions on seasonal forecasts. The inclusion of the Aquila et al. (2016) extensions to improve the radiative effects of large eruptions further enhances the suitability of GEOS-S2S for the assessment of the volcanic impact on seasonal prediction.

Data Availability Statement

FAIR data standards data availability: our paper GEOS-S2S-2 coupled forecast output data for P24, P60, and noP are presently available at: https://gmao.gsfc.nasa.gov/gmaoftp/gmaofcst/seasonal/GEOSS2S-2_1/, the full background ocean reanalysis is available at https://gmao.gsfc.nasa.gov/gmaoftp/gmaofcst/seasonal/GEOSS2S-2_1/OCN_DIR.

Acknowledgments
The GEOS-S2S model is developed via core funding to the GMAO from NASA's MAP program. Inclusion of aerosol modules is funded via GMAO core projects and the GEOS Chemistry-Climate Model effort. Computing was performed on NASA's High-Performance Computing machines at the NASA Center for Climate Simulation (Goddard Space Flight Center) and the NASA Computing Service (Ames Research Center).

References

Adams, J. B., Mann, M. E., & Ammann, C. M. (2003). Proxy evidence for an El Niño-like response to volcanic forcing. *Nature*, *426*, 274–278. https://doi.org/10.1038/nature02101

Aquila, V., Oman, L. D., Stolarski, R. S., Colarco, P. R., & Newman, P. A. (2012). Dispersion of the volcanic sulfate cloud from a Mount Pinatubo–like eruption. *Journal of Geophysical Research*, *117*, D06216. https://doi.org/10.1029/2011JD016968

Aquila, V., Swartz, W. H., Waugh, D. W., Colarco, P. R., Pawson, S., Polvani, L. M., & Stolarski, R. S. (2016). Isolating the roles of different forcing agents in global stratospheric temperature changes using model integrations with incrementally added single forcings. *Journal of Geophysical Research: Atmospheres*, *121*(13), 8067–8082. https://doi.org/10.1002/2015JD023841

Barahona, D., Molod, A., Bacmeister, J., Nenes, A., Gettelman, A., Morrison, H., et al. (2014). Development of two-moment cloud microphysics for liquid and ice within the NASA goddard earth observing system model (GEOS-5). *Geoscientific Model Development*, *7*(4), 1733–1766. https://doi.org/10.5194/gmd-7-1733-2014

Benedetti, A., & Vitart, F. (2018). Can the direct effect of aerosols improve subseasonal predictability? *Monthly Weather Review*, *146*(10), 3481–3498. https://doi.org/10.1175/MWR-D-17-0282.1

Bingen, C., Fussen, D., & Vanhellemont, F. (2004a). A global climatology of stratospheric aerosol size distribution parameters derived from SAGE II data over the period 1984-2000: 1. Methodology and climatological observations. *Journal of Geophysical Research: Atmospheres*, *109*(D6). https://doi.org/10.1029/2003jd003518

Bingen, C., Fussen, D., & Vanhellemont, F. (2004b). A global climatology of stratospheric aerosol size distribution parameters derived from SAGE II data over the period 1984-2000: 2. Reference data. *Journal of Geophysical Research: Atmospheres*, *109*(D6), D06202. https://doi.org/10.1029/2003jd003511

Bjerknes, J. (1969). Atmospheric teleconnections from the equatorial Pacific. *Monthly Weather Review*, *97*(3), 163–172. https://doi.org/10.1175/1520-0493(1969)097<0163:ATFTEP>2.3.CO;2

Broccoli, A. J., Dixon, K. W., Delworth, T. L., Knutson, T. R., Stouffer, R. J., & Zeng, F. (2003). Twentieth-century temperature and precipitation trends in ensemble climate simulations including natural and anthropogenic forcing. *Journal of Geophysical Research: Atmospheres*, *108*(D24), 4798. https://doi.org/10.1029/2003JD003812

Canty, T., Mascioli, N. R., Smarte, M. D., & Salawitch, R. J. (2013). An empirical model of global climate – Part 1: A critical evaluation of volcanic cooling. *Atmospheric Chemistry and Physics*, *13*(8), 3997–4031. https://doi.org/10.5194/acp-13-3997-2013

Carn, S. A., Yang, K., Prata, A. J., & Krotkov, N. A. (2015). Extending the long-term record of volcanic SO_2 emissions with the ozone mapping and profiler suite nadir mapper: OMPS volcanic SO_2 measurements. *Geophysical Research Letters*, *42*(3), 925–932. https://doi.org/10.1002/2014GL062437

Christy, J., Spencer, R., & Braswell, W. (2000). MSU tropospheric temperatures: Dataset construction and radiosonde comparisons. *Journal of Atmospheric And Oceanic Technology*, *17*, 1153–1170. https://doi.org/10.1175/1520-0426(2000)017<1153:MTTDCA>2.0.CO;2

Clement, A., Seager, R., Cane, M. A., & Zebiak, S. E. (1996). An ocean dynamical thermostat. *Journal of Climate*, *9*, 2190–2196. https://doi.org/10.1175/1520-0442(1996)009<2190:aodt>2.0.co;2

Colarco, P., da Silva, A., Chin, M., & Diehl, T. (2010). Online simulations of global aerosol distributions in the NASA GEOS-4 model and comparisons to satellite and ground-based aerosol optical depth. *Journal of Geophysical Research*, *115*, D14207. https://doi.org/10.1029/2009JD012820

Emile-Geay, J., Seager, R., Cane, M. A., Cook, E. R., & Haug, G. H. (2008). Volcanoes and ENSO over the past millennium. *Journal of Climate*, *21*(13), 3134–3148. https://doi.org/10.1175/2007JCLI1884.1

English, J. M., Toon, O. B., & Mills, M. J. (2013). Microphysical simulations of large volcanic eruptions: Pinatubo and Toba. *Journal of Geophysical Research*, *118*, 1880–1895. https://doi.org/10.1002/jgrd.50196

Gelaro, R., McCarty, W., Suárez, M. J., Todling, R., Molod, A., Takacs, L., et al. (2017). The modern-era retrospective analysis for research and applications, version 2 (MERRA-2). *Journal of Climate*, *30*(14), 5419–5454. https://doi.org/10.1175/JCLI-D-16-0758.1

Graf, H.-F., Kirchner, I., Robock, A., & Schult, I. (1993). Pinatubo eruption winter climate effects: Model versus observations. *Climate Dynamics*, *9*(2), 81–93. https://doi.org/10.1007/BF00210011

Griffies, S. (2012). *Elements of the modular ocean model (MOM)*. Retrieved from http://mdl-mom5.herokuapp.com/web/docs/project/MOM5_elements.pdf

Griffies, S. M., Gnanadesikan, A., Dixon, K. W., Dunne, J. P., Gerdes, R., Harrison, M. J., et al. (2005). Formulation of an ocean model for global climate simulations. *Ocean Science*, *1*, 45–79. https://doi.org/10.5194/os-1-45-2005

Gu, G., & Adler, R. F. (2011). Precipitation and temperature variations on the interannual time scale: Assessing the impact of ENSO and volcanic eruptions. *Journal of Climate*, *24*(9), 2258–2270. https://doi.org/10.1175/2010JCLI3727.1

Gu, G., Adler, R. F., Huffman, G. J., & Curtis, S. (2007). Tropical rainfall variability on interannual-to-interdecadal and longer time scales derived from the GPCP monthly product. *Journal of Climate*, *20*(15), 4033–4046. https://doi.org/10.1175/JCLI4227.1

Halpert, M. S., & Ropelewski, C. F. (1992). Surface temperature patterns associated with the southern oscillation. *Journal of Climate*, *5*(6), 577–593. https://doi.org/10.1175/1520-0442(1992)005<0577:STPAWT>2.0.CO;2

Huang, B., Xue, Y., Zhang, D., Kumar, A., & McPhaden, M. J. (2010). The NCEP GODAS ocean analysis of the tropical pacific mixed layer heat budget on seasonal to interannual time scales. *Journal of Climate*, *23*(18), 4901–4925. https://doi.org/10.1175/2010JCLI3373.1

Hunke, E. W., & Lipscomb, W. H. (2010). *CICE: The Los Alamos Sea Ice Model, documentation and software manual version 4.0*. Los Alamos National Laboratory.

Iles, C. E., Hegerl, G. C., Schurer, A. P., & Zhang, X. (2013). The effect of volcanic eruptions on global precipitation. *Journal of Geophysical Research: Atmospheres*, *118*(16), 8770–8786. https://doi.org/10.1002/jgrd.50678

Joseph, R., & Zeng, N. (2011). Seasonally modulated tropical drought induced by volcanic aerosol. *Journal of Climate*, *24*(8), 2045–2060. https://doi.org/10.1175/2009JCLI3170.1

Khodri, M., Izumo, T., Vialard, J., Janicot, S., Cassou, C., Lengaigne, M., et al. (2017). Tropical explosive volcanic eruptions can trigger El Niño by cooling tropical Africa. *Nature Communications*, *8*(1), 778. https://doi.org/10.1038/s41467-017-00755-6

Kirtman, B. P., Min, D., Infanti, J. M., Iii, J. L. K., Paolino, D. A., Zhang, Q., et al. (2014). *The North American multimodel ensemble. Phase-1 seasonal-to-interannual prediction. Phase-2 toward developing intraseasonal prediction* (Vol. 18).

Koster, R. D., Suarez, M. J., Ducharne, A., Stieglitz, M., & Kumar, P. (2000). A catchment-based approach to modeling land surface processes in a general circulation model. 1. Model structure. *Journal of Geophysical Research*, *105*(D20), 24809–24822. https://doi.org/10.1029/2000JD900327

Lean, J. L., & Rind, D. H. (2008). How natural and anthropogenic influences alter global and regional surface temperatures: 1889 to 2006. *Geophysical Research Letters*, *35*(18), L18701. https://doi.org/10.1029/2008GL034864

Lim, H.-G., Yeh, S.-W., Kug, J.-S., Park, Y.-G., Park, J.-H., Park, R., & Song, C.-K. (2016). Threshold of the volcanic forcing that leads the El Niño-like warming in the last millennium: Results from the ERIK simulation. *Climate Dynamics*, *46*(11–12), 3725–3736. https://doi.org/10.1007/s00382-015-2799-3

Mann, M. E., Cane, M. A., Zebiak, S. E., & Clement, A. (2005). Volcanic and solar forcing of the tropical Pacific over the past 1000 years. *Journal of Climate*, *18*, 447–456. https://doi.org/10.1175/JCLI-3276.1

McCormick, M. P., Thomason, L. W., & Trepte, C. R. (1995). Atmospheric effects of the Mt Pinatubo eruption. *Nature*, *373*(6513), 399–404. https://doi.org/10.1038/373399a0

McCormick, M. P., & Veiga, R. E. (1992). SAGE II measurements of early Pinatubo aerosols. *Geophysical Research Letters*, *19*(2), 155–158. https://doi.org/10.1029/91GL02790

McGregor, S., Khodri, M., Maher, N., Ohba, M., Pausata, F. S. R., & Stevenson, S. (2020). The effect of strong volcanic eruptions on ENSO. In *El Niño Southern Oscillation in a Changing Climate* (pp. 267–287). American Geophysical Union (AGU). https://doi.org/10.1002/9781119548164.ch12

McGregor, S., & Timmermann, A. (2011). The effect of explosive tropical volcanism on ENSO. *Journal of Climate*, *24*(8), 2178–2191. https://doi.org/10.1175/2010JCLI3990.1

McGregor, S., Timmermann, A., & Timm, O. (2010). A unified proxy for ENSO and PDO variability since 1650. *Climate of the Past*, *6*(1), 1–17. https://doi.org/10.5194/cp-6-1-2010

Meehl, G. A., Teng, H., Maher, N., & England, M. H. (2015). Effects of the Mount Pinatubo eruption on decadal climate prediction skill of Pacific sea surface temperatures. *Geophysical Research Letters*, *42*(24), 10840–10846. https://doi.org/10.1002/2015GL066608

Ménégoz, M., Bilbao, R., Bellprat, O., Guemas, V., & Doblas-Reyes, F. J. (2018). Forecasting the climate response to volcanic eruptions: Prediction skill related to stratospheric aerosol forcing. *Environmental Research Letters*, *13*(6), 064022. https://doi.org/10.1088/1748-9326/aac4db

Meyer, A., Folini, D., Lohmann, U., & Peter, T. (2016). Tropical temperature and precipitation responses to large volcanic eruptions: Observations and AMIP5 simulations. *Journal of Climate*, *29*(4), 1325–1338. https://doi.org/10.1175/JCLI-D-15-0034.1

Molod, A., Hackert, E., Vikhliaev, Y., Zhao, B., Barahona, D., Vernieres, G., et al. (2020). GEOS-S2S version 2: The GMAO high-resolution coupled model and assimilation system for seasonal prediction. *Journal of Geophysical Research: Atmospheres*, *125*(5), e2019JD031767. https://doi.org/10.1029/2019JD031767

Molod, A., Takacs, L., Suarez, M., & Bacmeister, J. (2015). Development of the GEOS-5 atmospheric general circulation model: Evolution from MERRA to MERRA2. *Geoscientific Model Development*, *8*, 1339–1356. https://doi.org/10.5194/gmd-8-1339-2015

Ohba, M., Shiogama, H., Yokohata, T., & Watanabe, M. (2013). Impact of strong tropical volcanic eruptions on ENSO simulated in a coupled GCM. *Journal of Climate*, *26*, 5169–5182. https://doi.org/10.1175/JCLI-D-12-00471.1

Pausata, F. S. R., Zanchettin, D., Karamperidou, C., Caballero, R., & Battisti, D. S. (2020). ITCZ shift and extratropical teleconnections drive ENSO response to volcanic eruptions. *Science Advances*, *6*(23), eaaz5006. https://doi.org/10.1126/sciadv.aaz5006

Polvani, L. M., Banerjee, A., & Schmidt, A. (2019). Northern Hemisphere continental winter warming following the 1991 Mt. Pinatubo eruption: Reconciling models and observations. *Atmospheric Chemistry and Physics*, *19*, 6351–6366. https://doi.org/10.5194/acp-19-6351-2019

Predybaylo, E., Stenchikov, G. L., Wittenberg, A. T., & Zeng, F. (2017). Impacts of a Pinatubo-size volcanic eruption on ENSO. *Journal of Geophysical Research: Atmospheres*, *122*(2), 925–947. https://doi.org/10.1002/2016JD025796

Putman, W. M., & Lin, S.-J. (2007). Finite-volume transport on various cubed-sphere grids. *Journal of Computational Physics*, *227*(1), 55–78. https://doi.org/10.1016/j.jcp.2007.07.022

Randles, C. A., da Silva, A. M., Buchard, V., Colarco, P. R., Darmenov, A., Govindaraju, R., et al. (2017). The MERRA-2 aerosol reanalysis, 1980 onward. Part I: System description and data assimilation evaluation. *Journal of Climate*, *30*(17), 6823–6850. https://doi.org/10.1175/JCLI-D-16-0609.1

Robock, A. (2000). Volcanic eruptions and climate. *Reviews of Geophysics*, *38*(2), 191–219. https://doi.org/10.1029/1998rg000054

Robock, A., & Liu, Y. (1994). The volcanic signal in goddard institute for space studies three-dimensional model simulations. *Journal of Climate*, *7*(2), 44–55. https://doi.org/10.1175/1520-0442(1994)007<0044:tvsigi>2.0.co;2

Robock, A., & Mao, J. (1992). Winter warming from large volcanic eruptions. *Geophysical Research Letters*, *19*(24), 2405–2408. https://doi.org/10.1029/92GL02627

Robock, A., & Mao, J. (1995). The volcanic signal in surface temperature observations. *Journal of Climate*, *8*, 1086–1103. https://doi.org/10.1175/1520-0442(1995)008<1086:tvsist>2.0.co;2

Santer, B. D., Bonfils, C., Painter, J. F., Zelinka, M. D., Mears, C., Solomon, S., et al. (2014). Volcanic contribution to decadal changes in tropospheric temperature. *Nature Geoscience*, *7*(3), 185–189. https://doi.org/10.1038/ngeo2098

Schneider, D. P., Ammann, C. M., Otto-Bliesner, B. L., & Kaufman, D. S. (2009). Climate response to large, high-latitude and low-latitude volcanic eruptions in the community climate system model. *Journal of Geophysical Research: Atmospheres*, *114*(D15), D15101. https://doi.org/10.1029/2008JD011222

Schubert, S., Borovikov, A., Lim, Y.-K., & Molod, A. (2019). *Ensemble generation strategies employed in the GMAO GEOS-S2S forecast system (Technical No. NASA/TM-2019-104606/Vol. 53)*. Retrieved from https://gmao.gsfc.nasa.gov/pubs/docs/Schubert1183.pdf

Soden, B. J. (2002). Global cooling after the eruption of Mount Pinatubo: A test of climate feedback by water vapor. *Science*, *296*(5568), 727–730. https://doi.org/10.1126/science.296.5568.727

Sprintall, J., & Tomczak, M. (1992). Evidence of the barrier layer in the surface layer of the tropics. *Journal of Geophysical Research*, *97*(C5), 7305. https://doi.org/10.1029/92JC00407

Stevenson, J. W., & Niiler, P. P. (1983). Upper ocean heat budget during the Hawaii-to-Tahiti shuttle experiment. *Journal of Physical Oceanography*, *13*, 1894–1907. https://doi.org/10.1175/1520-0485(1983)013<1894:UOHBDT>2.0.CO;2

Stevenson, S., Otto-Bliesner, B., Fasullo, J., & Brady, E. (2016). "El Niño Like" hydroclimate responses to last millennium volcanic eruptions. *Journal of Climate*, *29*(8), 2907–2921. https://doi.org/10.1175/JCLI-D-15-0239.1

Stockdale, T. N. (1997). Coupled ocean-atmosphere forecasts in the presence of climate drift. *Monthly Weather Review*, *125*, 809–818. https://doi.org/10.1175/1520-049310.1175/1520-0493(1997)125<0809:coafit>2.0.co;2

Thomason, L. W. (1992). Observations of a new SAGE II aerosol extinction mode following the eruption of Mt. Pinatubo. *Geophysical Research Letters*, *19*(21), 2179–2182. https://doi.org/10.1029/92GL02185

Thomason, L. W., Burton, S. P., Luo, B.-P., & Peter, T. (2008). SAGE II measurements of stratospheric aerosol properties at non-volcanic levels. *Atmospheric Chemistry and Physics*, *8*, 983–995. https://doi.org/10.5194/acp-8-983-2008

Trenberth, K. E., & Dai, A. (2007). Effects of Mount Pinatubo volcanic eruption on the hydrological cycle as an analog of geoengineering. *Geophysical Research Letters*, *34*(15), L15702. https://doi.org/10.1029/2007GL030524

Wang, T., Guo, D., Gao, Y., Wang, H., Zheng, F., Zhu, Y., et al. (2018). Modulation of ENSO evolution by strong tropical volcanic eruptions. *Climate Dynamics*, *51*(7–8), 2433–2453. https://doi.org/10.1007/s00382-017-4021-2

Yang, W., Vecchi, G. A., Fueglistaler, S., Horowitz, L. W., Luet, D. J., Muñoz, Á. G., et al. (2019). Climate impacts from large volcanic eruptions in a high-resolution climate model: The importance of forcing structure. *Geophysical Research Letters*, *46*(13), 7690–7699. https://doi.org/10.1029/2019GL082367

Zebiack, S. E., & Cane, M. A. (1987). A model El Niño-Southern Oscillation. *Monthly Weather Review*, *115*, 2262–2278. https://doi.org/10.1175/1520-0493(1987)115<2262:AMENO>2.0.CO;2

Zuo, M., Man, W., Zhou, T., & Guo, Z. (2018). Different Impacts of northern, tropical, and southern volcanic eruptions on the tropical Pacific SST in the last millennium. *Journal of Climate*, *31*(17), 6729–6744. https://doi.org/10.1175/JCLI-D-17-0571.1